Prediction of superconducting properties of CaB_2 using anisotropic Eliashberg theory

Hyoung Joon Choi,[1,*] Steven G. Louie,[2,3] and Marvin L. Cohen[2,3]
[1]*Department of Physics and IPAP, Yonsei University, Seoul 120-749, Korea*
[2]*Department of Physics, University of California, Berkeley, California 94720, USA*
[3]*Materials Sciences Division, Lawrence Berkeley National Laboratory, Berkeley, California 94720, USA*
(Received 14 June 2009; published 7 August 2009)

Superconducting properties of hypothetical simple hexagonal CaB_2 are studied using the fully anisotropic Eliashberg formalism based on electronic and phononic structures and electron-phonon interactions, which are obtained from *ab initio* pseudopotential density-functional calculations. The superconducting transition temperature T_c, the superconducting energy gap $\Delta(\mathbf{k})$ on the Fermi surface, and the specific heat are obtained and compared with corresponding properties of MgB_2. Our results suggest that CaB_2 will have a higher T_c and a stronger two-gap nature, with a larger $\Delta(\mathbf{k})$ in the σ bands but a smaller $\Delta(\mathbf{k})$ in the π bands than MgB_2.

DOI: 10.1103/PhysRevB.80.064503 PACS number(s): 74.20.Fg, 71.15.Mb, 74.70.Ad, 61.50.Ah

The discovery of superconductivity in MgB_2 (Ref. 1) with its remarkable superconducting transition temperature T_c as high as 39 K has triggered many investigations of related materials including various binaries: BeB_2,[2–4] CaB_2,[3–7] NaB_2,[7] SrB_2,[4,7] CuB_2,[8] ZrB_2,[7,9] TaB_2,[7,10] OsB_2,[11] ScB_2,[3,7] YB_2,[3,7] $MgBe_2$,[8] MgB_4,[4] and LiB,[12] and ternaries: CaBeSi,[2] LiBC,[4,13–16] NaBC,[16] $MgB_{2-x}C_x$,[3,5] $Mg_{1-x}Ca_xB_2$,[3,5,17,18] $Mg_{1-x}Li_xB_2$,[3,5] $Mg_{1-x}Na_xB_2$,[3,5] $MgBe_xB_{2-x}$,[5,8] $CuB_{2-x}C_x$,[8] MgB_2C_2,[4] and $Be_2B_xC_{1-x}$.[19] For these compounds, their structural, electronic, and superconducting properties are studied experimetally[9–11,15,17,18] and theoretically.[2–8,10,12–16,19] The structural stabilities of the existing and hypothetical compounds are studied extensively as well.[7,20] Even with these efforts, however, the highest T_c observed experimentally in these compounds is still that of MgB_2. There have been theoretical predictions of T_c's higher than 39 K, for example, $T_c \sim 50$ K in $CuB_{2-x}C_x$ (Ref. 8) and $T_c \sim 100$ K (Ref. 13) and 65 K (Ref. 14) in hole-doped LiBC.

One of the interesting candidates for a higher T_c is the hypothetical simple hexagonal CaB_2, with the same crystal symmetry as MgB_2, with all Mg atoms being replaced by Ca atoms. First-principles calculations predict that the simple hexagonal CaB_2 should have a greater unit cell (both a and c lattice constants are longer) and a much larger value for the density of states (DOS) at the Fermi energy (E_F) than MgB_2.[3–7] Both features are favorable for a higher T_c, since MgB_2 is found to have a positive dependence of T_c on the unit-cell volume[21] and more generally, a larger DOS at E_F can result in a greater electron-phonon coupling constant. Although CaB_2 is an attractive candidate for superconductivity, it has not been synthesized as yet, nor has it been extensively studied theoretically for superconductivity. Since the Fermi surface of CaB_2 is predicted to consist of multiple sheets similar to those in MgB_2,[3–6] it will be necessary to use the anisotropic Eliashberg theory to deal with the effects of possible variations in the superconducting energy gap on the Fermi surface as in the case of MgB_2.[22,23]

In this paper, we perform density-functional *ab initio* pseudopotential calculations to determine the lattice constants of the hypothetical simple hexagonal phase of CaB_2, and we calculate its electronic structure, phonon spectrum, and electron-phonon properties. From these material properties, we construct the fully anisotropic Eliashberg equations to obtain the superconducting properties such as T_c, the momentum-dependent superconducting energy gap $\Delta(\mathbf{k},T)$, and the specific heat as functions of temperature T. These results predict that CaB_2 has a higher T_c than MgB_2 and a larger difference between the superconducting energy gap in the σ and π bands when compared with MgB_2.

We consider the hypothetical simple hexagonal CaB_2 shown in Fig. 1. The atomic structure has exactly the same symmetry as MgB_2, having one Ca and two B atoms in a unit cell. We determine the lattice constants a and c by minimizing the total energy of the system obtained from first-principles pseudopotential density-functional calculations.[24,25] In the calculations, plane waves of energy up to 60 Ry are used to expand the electronic wave functions, norm-conserving pseudopotentials[26] are used to describe the electron-ion interactions, and the local-density approximation is employed to deal with the electron-electron interactions effectively. In more detail, we use the partial-core correction[27] for the Ca pseudopotential, Ceperley-Alder exchange-correlation energy[28] of the Perdew-Zunger parameterization,[29] a $12\times12\times12$ k-point grid to evaluate the self-consistent electron density, and a $18\times18\times12$ k-point grid for Fermi-surface properties.

For simple hexagonal CaB_2, the calculated lattice constants at ambient pressure are $a=3.185$ Å and $c=4.060$ Å.

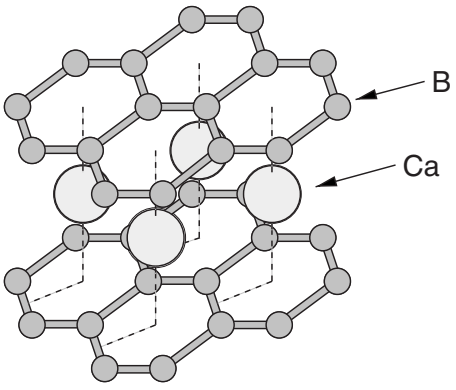

FIG. 1. Atomic structure of hypothetical simple hexagonal CaB_2. The simple hexagonal unit cell contains one Ca and two B atoms.

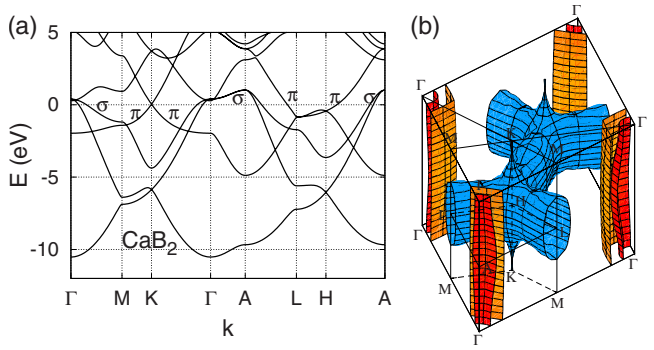

FIG. 2. (Color online) Electronic structure of CaB_2: (a) electronic band structure and (b) the Fermi surface. In (b), the cylindrical [red (dark gray) and orange (light gray)] sheets along the $\Gamma-A-\Gamma$ line are of hole type, and the connected [blue (light gray)] sheet along H–L lines is of electron type.

Thus the c/a ratio is 1.27. Compared with theoretical values for MgB_2 (which are $a=3.07$ Å and $c=3.57$ Å, with $c/a=1.16$), a in CaB_2 is 4% greater and c is 14% greater. To check the ratio of c/a at high pressure, we obtain the lattice constants at 30 GPa, which are $a=3.014$ Å and $c=3.842$ Å. Thus, the c/a ratio is still 1.27 at this pressure. The obtained $c/a=1.27$ is larger than 1.165 known as the maximal c/a ratio of existing diborides,[30] and this is in agreement with previous calculations.[3–7] Since the hexagonal CaB_2 has not been synthesized successfully, its formation energy and stability have been studied theoretically.[3,7,20] Hexagonal CaB_2 is predicted to be stable with respect to hcp Ca and rhombohedral B (α-B_{12}),[3] but unstable to a phase separation into fcc Ca and CaB_6,[7] and less stable than δ-CaB_2 phase.[20] As reported theoretically, hexagonal CaB_2 may not be the lowest phase energetically, but our frozen-phonon calculations at high-symmetry points, which will be presented below, do not show any structural instability from the simple hexagonal phase.

With the optimized lattice constants, we perform first-principles electronic structure calculations. Figure 2 shows the obtained band structure along the high-symmetry lines and the Fermi surface. Overall, the band structure of CaB_2 is similar to MgB_2. In Fig. 2(a), the σ and the π bands are from the boron sp^2 and p_z orbitals, respectively. The full bandwidth of the σ bands is reduced substantially, compared with MgB_2, because of the larger B-B bond length. As in the case of MgB_2, the Fermi energy in CaB_2 is lower than the top of the σ bands, producing two cylindrical hole-type sheets along the $\Gamma-A$ line [Fig. 2(b)]. While the hole-type sheets are close to those in MgB_2 qualitatively, the electron-type sheet from the π bands in CaB_2 is quite different from the one in MgB_2. In MgB_2, the π bands are above E_F at the M and K points; however, in CaB_2, they are below E_F. Thus, CaB_2 has only one electron-type Fermi surface from the π bands along H–L lines [Fig. 2(b)], missing the Fermi surface along the $K-L$ line that is present in MgB_2. Hence, as shown in Fig. 2(b), the Fermi surface in CaB_2 consists of three sheets: two hole-type cylindrical ones along $\Gamma-A$ lines and one electron-type along H–L lines. The density of states at the Fermi level in CaB_2 is 0.96 states/eV per f.u., which is much larger than 0.69 states/eV for MgB_2. The contributions

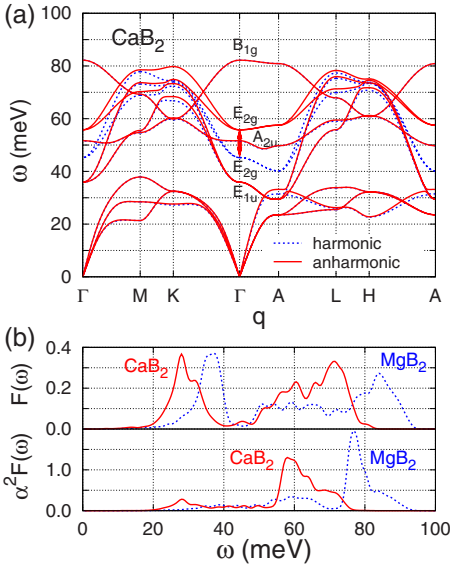

FIG. 3. (Color online) Phonon dispersion relations and electron-phonon interactions in CaB_2. (a) Dashed (blue) lines are the phonon dispersions within the harmonic approximation and solid (red) lines are those considering anharmonicity in the frozen-phonon calculations. As in the case of MgB_2, the doubly degenerate E_{2g} mode along the $\Gamma-A$ line is highly affected by anharmonicity. In the harmonic case, the frequency of the E_{2g} mode is even lower than the A_{2u} mode, but the former becomes higher than the latter in the anharmonic case. (b) Phonon DOS $F(\omega)$ in meV^{-1} and the Eliashberg function $\alpha^2F(\omega)$ including anharmonic effects on the phonon frequencies. Solids (red) lines are the phonon DOS and the Eliashberg function in CaB_2. Dashed (blue) lines are those in MgB_2 drawn for comparison.

of the three sheets of the Fermi surface to the DOS at E_F are 12%, 32%, and 56% from the inner and outer hole-type sheets and the electron-type sheet, respectively. Our results for the band structures are in good agreement with the results using the full-potential linear muffin-tin orbital method.[3,5]

To consider electron-phonon interactions, we calculate the phonon structures in CaB_2 based on the frozen-phonon method. In the first step, phonon frequencies and polarizations are obtained at high-symmetry points of the Brillouin zone (BZ) by frozen-phonon methods, and then interpolated to the full Brillouin zone by interpolating the dynamical matrix. In the frozen-phonon calculations, we extract quadratic and higher-order dependences of the total energy on atomic displacements, and calculate harmonic and anharmonic phonon frequencies with and without using the harmonic approximation.

Figure 3(a) shows the calculated phonon dispersions along the high-symmetry lines, with and without anharmonicity. The phonon frequencies are calculated by constructing the dynamical matrices at the high-symmetry points and interpolating them along the high-symmetry lines. In our frozen-phonon calculations, the increase in the total energy with boron displacements are highly anharmonic for E_{2g} modes (the B-B bond-stretching modes) at the Γ and A points. This is consistent with the reported large anharmonicity at Γ in CaB_2.[31] We find that the E_{2g} frequency is 45.2 meV in the harmonic case and 55.8 meV in the anharmonic

case, both of which are substantially lower than those in MgB_2. All the phonon frequencies at the high-symmetry points are positive, and therefore, do not indicate structural instabilities.

The upper panel in Fig. 3(b) shows the phonon density of states obtained by interpolating the dynamical matrix throughout the Brillouin zone with anharmonicity included. Compared with MgB_2, the phonons in CaB_2 have lower frequencies. Phonon modes associated with Ca atoms should have lower frequencies because of heavier atomic mass of Ca relative to Mg. In addition, phonon modes associated with B atoms also have lower frequencies because of the elongation of B-B bonds.

We calculate the momentum-dependent Eliashberg function $\alpha^2F(\mathbf{k},\mathbf{k}',\omega)$ from the difference in the self-consistent potential with and without frozen phonons, using the anharmonic phonon frequencies, and then take the average on the Fermi surface to obtain the isotropic Eliashberg function $\alpha^2F(\omega)$, as shown in the lower panel in Fig. 3(b). From $\alpha^2F(\omega)$, we can evaluate the average electron-phonon coupling constant $\lambda=2\int d\omega\alpha^2F(\omega)/\omega$ and the logarithmically averaged phonon frequency $\omega_{\ln}=\exp[(2/\lambda)\int d\omega\alpha^2F(\omega)\ln\omega/\omega]$. This gives $\lambda=0.69$ and $\omega_{\ln}=50$ meV, respectively. The value of λ is 13% larger and $\omega_{\ln}$ is 34% smaller than those for MgB_2.

We obtain the superconducting properties in CaB_2 using the fully anisotropic Eliashberg formalism.[22,32] The anisotropic Eliashberg equations at imaginary frequencies are given as

$$Z(\mathbf{k},i\omega_n)=1+f_n s_n\sum_{\mathbf{k}'n'}W_{\mathbf{k}'}\lambda(\mathbf{k},\mathbf{k}',n-n')\times\frac{\omega_{n'}}{\sqrt{\omega_{n'}^2+\Delta(\mathbf{k}',i\omega_{n'})^2}},\quad(1)$$

$$Z(\mathbf{k},i\omega_n)\Delta(\mathbf{k},i\omega_n)=\pi T\sum_{\mathbf{k}'n'}W_{\mathbf{k}'}[\lambda(\mathbf{k},\mathbf{k}',n-n')-\mu^*(\omega_c)]\times\frac{\Delta(\mathbf{k}',i\omega_{n'})}{\sqrt{\omega_{n'}^2+\Delta(\mathbf{k}',i\omega_{n'})^2}},\quad(2)$$

where $\omega_n=(2n+1)\pi T$ is the Fermionic Matsubara frequency at temperature T, $Z(\mathbf{k},i\omega_n)$ and $\Delta(\mathbf{k},i\omega_n)$ are the momentum-dependent renormalization function and the gap function, respectively, and $\lambda(\mathbf{k},\mathbf{k}',n)$ represents the momentum-dependent electron-phonon interactions. Definitions of symbols and detail of the numerical method are described in Refs. 23, 33, and 34. Here, we assume that the Coulomb pseudopotential μ^* is isotropic, since its momentum dependence is not as strong as that of the electron-phonon interaction,[35–37] and assume $\mu^*(\omega_c)=0.12$ for the cutoff frequency $\omega_c=0.5$ eV, as assumed for MgB_2.[22,23]

We obtain T_c by finding the highest T at which the anisotropic Eliashberg equations [Eqs. (1) and (2)] have a nontrivial solution for $\Delta(\mathbf{k})$. With the assumed value of $\mu^*(\omega_c)=0.12$, we obtain $T_c=48$ K, which is about 10 K higher than that of MgB_2. To check the sensitivity of T_c to μ^*, we also consider $\mu^*(\omega_c)=0.10$ and 0.14, obtaining $T_c=50$ and 46 K, respectively. Thus, we can expect a higher T_c in CaB_2 than in MgB_2 even in the case of relative large μ^*.

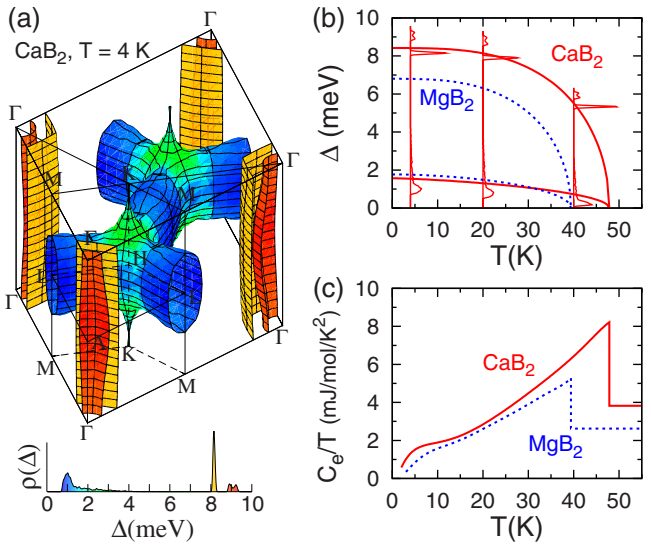

FIG. 4. (Color online) Superconducting properties in CaB_2. (a) Superconducting energy gap $\Delta(\mathbf{k})$ on the Fermi surface at 4 K plotted using a color scale. The lower panel shows the distribution $\rho(\Delta)$ of the values of the energy gap as well as the color scale for the size of the energy gap. (b) Temperature dependence of the superconducting energy gaps [solid (red) lines]. Dashed (blue) lines are the superconducting energy gaps in MgB_2 drawn for comparision. Vertical lines represent the distributions of $\Delta(\mathbf{k})$ in CaB_2 at 4, 20, and 40 K. Curves are fit to the separate averages, Δ_σ and Δ_π, where the average Δ_π is greater than the peak energy of $\rho(\Delta)$ in (a) because of the high-energy tail of $\rho(\Delta)$ [green part in (a)]. (c) The specific heat C_e over T of CaB_2 [solid (red) line]. The dashed (blue) line is C_e/T of MgB_2 drawn for comparision. Anharmonic effects on the phonon frequencies are considered in all calculations of the superconducting properties.

With Eqs. (1) and (2), and their analytic continuations to the real-frequency axis, we calculate the superconducting properties below T_c. Figure 4(a) shows the calculated superconducting energy gap on the Fermi surface at $T=4$ K, where the average values of $\Delta(\mathbf{k})$ on the three sheets of the Fermi surface are well separated from one another and they are 9.1, 8.2, and 1.5 meV, respectively, with the average on the two hole-type sheets being 8.4 meV. As shown in Fig. 4(b), when compared with MgB_2, the average value Δ_σ of $\Delta(\mathbf{k})$ on the σ bands (the hole-type sheets) is substantially larger but Δ_π for the π bands is slightly smaller at low T, indicating an enhanced two-gap nature for CaB_2. Figure 4(c) shows the calculated electronic specific heat as a function of temperature. Because of the higher DOS at E_F and the larger λ, the normal-state specific heat C_N above T_c is expected to be larger in CaB_2 ($C_N=\gamma_n T$ with $\gamma_n=3.82$ mJ mol^{-1} K^{-2}) than in MgB_2 ($\gamma_n=2.62$ mJ mol^{-1} K^{-2}). In addition, since Δ_π in CaB_2 is smaller in magnitude than in MgB_2, the specific heat at $T<10$ K has a bigger hump in CaB_2.

To summarize, we obtained the lattice constants, the electronic and phononic structures, and electron-phonon interac-

tions in hypothetical simple hexagonal CaB_2 using first-principles calculations. We then calculated the superconducting transition temperature T_c, the superconducting energy gap $\Delta(\mathbf{k},T)$, and the specific heat using the fully anisotropic Eliashberg formalism. The obtained Fermi surface in CaB_2 consists of three sheets rather than four as in MgB_2, and the phonon frequencies are lower than in MgB_2. A substantially higher T_c is predicted for hexagonal CaB_2, and furthermore, the multiple superconducting energy-gap feature is expected to be enhanced in CaB_2, with larger Δ_σ and smaller Δ_π than in MgB_2.

This work was supported by the KRF (Grant No. KRF-2007-314-C00075), by the KOSEF under Grant No. R01-2007-000-20922-0, by NSF under Grant No. DMR07-05941, and by the Director, Office of Science, Office of Basic Energy Sciences, Materials Sciences and Engineering Division, U.S. Department of Energy under Contract No. DE-AC02-05CH11231. Computational resources have been provided by KISTI Supercomputing Center (Project No. KSC-2008-S02-0004), NSF through TeraGrid resources at SDSC, and DOE at Lawrence Berkeley National Laboratory's NERSC facility.

*h.j.choi@yonsei.ac.kr

[1] J. Nagamatsu, N. Nakagawa, T. Muranaka, Y. Zenitani, and J. Akimitsu, Nature (London) **410**, 63 (2001).
[2] G. Satta, G. Profeta, F. Bernardini, A. Continenza, and S. Massidda, Phys. Rev. B **64**, 104507 (2001).
[3] N. I. Medvedeva, A. L. Ivanovskii, J. E. Medvedeva, and A. J. Freeman, Phys. Rev. B **64**, 020502(R) (2001).
[4] P. Ravindran, P. Vajeeston, R. Vidya, A. Kjekshus, and H. Fjellvåg, Phys. Rev. B **64**, 224509 (2001).
[5] N. I. Medvedeva, J. E. Medvedeva, A. L. Ivanovskii, V. G. Zubkov, and A. J. Freeman, Pis'ma Zh. Eksp. Teor. Fiz. **73**, 378 (2001) [JETP Lett. **73**, 336 (2001)].
[6] S. V. Okatov, A. L. Ivanovskii, Y. E. Medvedeva, and N. I. Medvedeva, Phys. Status Solidi B **225**, R3 (2001).
[7] T. Oguchi, J. Phys. Soc. Jpn. **71**, 1495 (2002).
[8] M. J. Mehl, D. A. Papaconstantopoulos, and D. J. Singh, Phys. Rev. B **64**, 140509(R) (2001).
[9] V. A. Gasparov, N. S. Sidorov, I. I. Zver'kova, and M. P. Kulakov, JETP Lett. **73**, 532 (2001).
[10] H. Rosner, W. E. Pickett, S.-L. Drechsler, A. Handstein, G. Behr, G. Fuchs, K. Nenkov, K.-H. Müller, and H. Eschrig, Phys. Rev. B **64**, 144516 (2001).
[11] Y. Singh, A. Niazi, M. D. Vannette, R. Prozorov, and D. C. Johnston, Phys. Rev. B **76**, 214510 (2007).
[12] M. Calandra, A. N. Kolmogorov, and S. Curtarolo, Phys. Rev. B **75**, 144506 (2007).
[13] H. Rosner, A. Kitaigorodsky, and W. E. Pickett, Phys. Rev. Lett. **88**, 127001 (2002).
[14] J. K. Dewhurst, S. Sharma, C. Ambrosch-Draxl, and B. Johansson, Phys. Rev. B **68**, 020504(R) (2003).
[15] A. Lazicki, C.-S. Yoo, H. Cynn, W. J. Evans, W. E. Pickett, and J. Olamit, K. Liu, and Y. Ohishi, Phys. Rev. B **75**, 054507 (2007).
[16] S. Lebègue, B. Arnaud, P. Rabiller, M. Alouani, and W. E. Pickett, Europhys. Lett. **68**, 846 (2004).
[17] Y. Sun, D. Yu, Z. Liu, T. Wang, J. He, J. Xiang, D. Zheng, and Y. Tian, Supercond. Sci. Technol. **20**, 261 (2007).
[18] Y. Sun, D. Yu, Z. Liu, J. He, X. Zhang, Y. Tian, J. Xiang, and D. Zheng, Appl. Phys. Lett. **90**, 052507 (2007).
[19] J. E. Moussa, J. Noffsinger, and M. L. Cohen, Phys. Rev. B **78**, 104506 (2008).
[20] A. N. Kolmogorov and S. Curtarolo, Phys. Rev. B **74**, 224507 (2006).
[21] C. Buzea and T. Yamashita, Supercond. Sci. Technol. **14**, R115 (2001) and references therein.
[22] H. J. Choi, D. Roundy, H. Sun, M. L. Cohen, and S. G. Louie, Nature (London) **418**, 758 (2002).
[23] H. J. Choi, D. Roundy, H. Sun, M. L. Cohen, and S. G. Louie, Phys. Rev. B **66**, 020513(R) (2002).
[24] J. Ihm, A. Zunger, and M. L. Cohen, J. Phys. C **12**, 4409 (1979).
[25] M. L. Cohen, Phys. Scr. **T1**, 5 (1982).
[26] N. Troullier and J. L. Martins, Phys. Rev. B **43**, 1993 (1991).
[27] S. G. Louie, S. Froyen, and M. L. Cohen, Phys. Rev. B **26**, 1738 (1982).
[28] D. M. Ceperley and B. J. Alder, Phys. Rev. Lett. **45**, 566 (1980).
[29] J. P. Perdew and A. Zunger, Phys. Rev. B **23**, 5048 (1981).
[30] B. Aronsson, T. Lundstrom, and S. Rundqvist, *Refractory Borides, Silicides and Phosphides* (Methuen, London, 1965).
[31] T. Yildirim, O. Gulseren, J. W. Lynn, C. M. Brown, T. J. Udovic, Q. Huang, N. Rogado, K. A. Regan, M. A. Hayward, J. S. Slusky, T. He, M. K. Haas, P. Khalifah, K. Inumaru, and R. J. Cava, Phys. Rev. Lett. **87**, 037001 (2001).
[32] P. B. Allen and B. Mitrović, in *Solid State Physics*, edited by H. Ehrenreich, F. Seitz, and D. Turnbull (Academic, New York, 1982), Vol. 37, p. 1.
[33] H. J. Choi, M. L. Cohen, and S. G. Louie, Physica C **385**, 66 (2003).
[34] H. J. Choi, M. L. Cohen, and S. G. Louie, Phys. Rev. B **73**, 104520 (2006).
[35] C.-Y. Moon, Y.-H. Kim, and K. J. Chang, Phys. Rev. B **70**, 104522 (2004).
[36] I. I. Mazin, O. K. Andersen, O. Jepsen, A. A. Golubov, O. V. Dolgov, and J. Kortus, Phys. Rev. B **69**, 056501 (2004).
[37] H. J. Choi, D. Roundy, H. Sun, M. L. Cohen, and S. G. Louie, Phys. Rev. B **69**, 056502 (2004).